

STACKING THE INVISIBLES: A GUIDED SEARCH FOR LOW-LUMINOSITY MILKY WAY SATELLITES

BRANIMIR SESAR^{1,2,6}, SOPHIANNA R. BANHOLZER¹, JUDITH G. COHEN¹, NICOLAS F. MARTIN^{2,4}, CARL J. GRILLMAIR³,
DAVID LEVITAN¹, RUSS R. LAHER³, ERAN O. OFEK⁵, JASON A. SURACE³, SHRINIVAS R. KULKARNI¹, THOMAS A. PRINCE¹,
AND HANS-WALTER RIX²

Draft version November 2, 2021

ABSTRACT

Almost every known low-luminosity Milky Way dwarf spheroidal (dSph) satellite galaxy contains at least one RR Lyrae star. Assuming that a fraction of distant ($60 < d_{helio} < 100$ kpc) Galactic halo RR Lyrae stars are members of yet to be discovered low-luminosity dSph galaxies, we perform a *guided* search for these low-luminosity dSph galaxies. In order to detect the presence of dSph galaxies, we combine stars selected from more than 123 sightlines centered on RR Lyrae stars identified by the Palomar Transient Factory. We find that this method is sensitive enough to detect the presence of Segue 1-like galaxies ($M_V = -1.5^{+0.6}_{-0.8}$, $r_h = 30$ pc) even if only ~ 20 sightlines were occupied by such dSph galaxies. Yet, when our method is applied to the SDSS DR10 imaging catalog, no signal is detected. An application of our method to sightlines occupied by pairs of close (< 200 pc) horizontal branch stars, also did not yield a detection. Thus, we place upper limits on the number of low-luminosity dSph galaxies with half-light radii from 30 pc to 120 pc, and in the probed volume of the halo. Stronger constraints on the luminosity function may be obtained by applying our method to sightlines centered on RR Lyrae stars selected from the Pan-STARRS1 survey, and eventually, from LSST. In the Appendix, we present spectroscopic observations of an RRab star in the Boötes 3 dSph and a light curve of an RRab star near the Boötes 2 dSph.

Subject headings: stars: variables: RR Lyrae — Galaxy: halo — Galaxy: structure — galaxies: dwarf

1. INTRODUCTION

One of the predictions of the Λ Cold Dark Matter (ACDM) model is an abundance of low-mass dark matter subhalos orbiting their host galaxies at the present epoch (Klypin et al. 1999; Moore et al. 1999). Taking into account sensitivity limits of searches based on the Sloan Digital Sky Survey data (SDSS; York et al. 2000), Tollerud et al. (2008) predict “that there should be between ~ 300 and ~ 600 satellites within 400 kpc of the Sun that are brighter than the faintest known dwarf galaxies.” (One of the least luminous known Milky Way satellite dwarf galaxies is Segue 1 (Belokurov et al. 2007) with $M_V = -1.5^{+0.6}_{-0.8}$ (Martin et al. 2008).) While Milky Way satellites brighter than $M_V \sim -4$ have all likely been discovered in the SDSS footprint within ~ 100 kpc, less luminous satellites ($M_V \gtrsim -4$) may exist beyond 45 kpc from the Sun, just below the detection limit of current surveys (e.g., see Figure 10 of Koposov et al. 2008).

To illustrate the difficulties of detecting, for example, a faint Segue 1-like satellite at 60 kpc, consider the fact that Segue 1 has only 8 stars above the main sequence turnoff (2 horizontal branch (HB) stars and 6 red giant branch (RGB) stars; Simon et al. 2011). At 60 kpc, an imaging survey with a faint limit of $r \sim 22.5$ (e.g.,

SDSS or PS1; Metcalfe et al. 2013) could at best see these 8 stars in the satellite galaxy. Identifying these 8 stars as a statistically significant spatial overdensity of sources in the sea of foreground stars and background galaxies, is likely out of reach even for the most recent detection algorithms (e.g., Walsh et al. 2009⁷, Martin et al. 2013) and current datasets, unless accurate distances or additional data are available (e.g., kinematics, chemical abundances).

While low-luminosity (e.g., similar to Segue 1) Milky Way satellites may not be detectable in *blind* searches until surveys such as the Large Synoptic Survey Telescope (LSST; Ivezić et al. 2008) provide deeper multi-color imaging covering large areas on the sky, they may be detectable in *guided* searches. For example, if one had an indication of a faint satellite’s location, one could do targeted deep imaging to reach below the satellite’s main sequence turnoff and achieve a reliable detection.

We argue that *ab*-type RR Lyrae stars (hereafter, RRab; Smith 2004), located in the outer Galactic halo (i.e., at galactocentric distances $R_{GC} > 30$ kpc), are the best practical indicators of the locations where distant and low-luminosity Milky Way satellites may exist. As Table 4 of Boettcher et al. (2013) and our Appendix A show, *almost every low-luminosity ($M_V \gtrsim -8$) Milky Way dwarf satellite galaxy has at least one RRab star*. Even the least luminous of Milky Way dwarf satellites, Segue 1, has one RR Lyrae star (Simon et al. 2011). This finding shows that RR Lyrae stars are plausible tracers of even the least luminous and most metal-poor Milky Way dwarf satellites.

RR Lyrae stars have several properties that make them

¹ Division of Physics, Mathematics and Astronomy, California Institute of Technology, Pasadena, CA 91125, USA

² Max Planck Institute for Astronomy, Königstuhl 17, D-69117 Heidelberg, Germany

³ Spitzer Science Center, California Institute of Technology, Pasadena, CA 91125, USA

⁴ Observatoire Astronomique de Strasbourg, Université de Strasbourg, F-67000 Strasbourg, France

⁵ Benozio Center for Astrophysics, Weizmann Institute of Science, 76100 Rehovot, Israel

⁶ Corresponding author: bsesar@mpia.de

⁷ Whom we thank for inspiring the title of this manuscript.

useful as tracers of halo structures. First, they are bright stars ($M_r = 0.6$ mag at $[\text{Fe}/\text{H}] = -1.5$ dex) that can be detected at large distances (5-120 kpc for $14 < r < 21$). Second, distances of RRab stars measured from optical data are precise to $\sim 6\%$ (Sesar et al. 2013b) (vs., e.g., 15% for K giants; Xue et al. 2014), and can be improved to better than 3% using infrared data (Klein et al. 2011). And finally, RRab stars have distinct, sawtooth shaped light curves which make them easy to identify given multi-epoch observations (peak-to-peak amplitudes of ~ 1 mag in the r -band and periods of ~ 0.6 days).

In this paper, we describe a statistical approach that amounts to a guided search for low-luminosity Milky Way dwarf satellite galaxies, using distant ($R_{GC} > 60$ kpc) RRab stars as indicators of their position. The sample of RRab stars is described in Section 2). Instead of attempting to detect an overdensity of sources (i.e., a low-luminosity dSph) at a particular position and distance indicated by an RRab star, we search for evidence of faint dSphs in the ensemble color-magnitude diagrams, stacked at the positions and distances of RR Lyrae stars. Our detection method is described in Sections 3.1 and 3.2, and its sensitivity is measured in Section 3.3. The application of our method to SDSS DR10 imaging data (Ahn et al. 2014) is described in Section 4, and the results are discussed in Section 5.

2. RR LYRAE STARS

RRab stars used in this work were selected by an automated classification algorithm that uses imaging data provided by the Palomar Transient Factory survey (PTF). Below we briefly describe the PTF survey and the RR Lyrae selection procedure.

The PTF⁸ (Law et al. 2009; Rau et al. 2009) is a synoptic survey designed to explore the transient sky. The project utilizes the 48-inch Samuel Oschin Schmidt Telescope on Mount Palomar. Each PTF image covers 7.26 deg^2 with a pixel scale of $1.01''$. The typical PTF cadence consists of two 60-sec exposures separated by ~ 1 hour and repeated every one to five days. By June 2013, PTF observed $\sim 11,000 \text{ deg}^2$ of sky at least 25 times in the Mould- R filter⁹ (hereafter, the R -band filter), and about 2200 deg^2 in the SDSS g' filter. PTF photometry is calibrated to an accuracy of about 0.02 mag (Ofek et al. 2012a,b) and light curves have relative precision of better than 10 mmag at the bright end, and about 0.2 mag at the survey limiting magnitude of $R = 20.6$ mag. The relative photometry algorithm is described in Ofek et al. (2011, see their Appendix A).

Briefly, to select RR Lyrae stars from PTF we first searched for variable PTF sources that have SDSS colors consistent with colors of RR Lyrae stars (Equations 6 to 9 of Sesar et al. 2010). A period-finding algorithm was then applied to light curves of color-selected objects, and objects with periods in the range 0.2-0.9 days were kept. Light curves were phased (period-folded) and SDSS r -band RR Lyrae light curve templates (constructed by Sesar et al. 2010) were fitted to the phased data. A Random Forest classifier, trained on the sample of RR

Table 1
Positions and distances of RR Lyrae stars

R.A. (deg)	Dec (deg)	Helio. distance ^a (kpc)
1.242728	3.098036	88.8
1.682986	21.730624	72.9
3.939427	-5.579277	78.4

Note. — Table 1 is published in its entirety in the electronic edition of the Journal. A portion is shown here for guidance regarding its form and content.

^a Calculated assuming $M_r = 0.6$ as the absolute magnitude of RR Lyrae stars in the PTF R -band. The fractional uncertainty in distance is 6%.

Lyrae stars identified in SDSS Stripe 82 (Sesar et al. 2010), was then used to classify candidate RR Lyrae stars observed by PTF (Banholzer et al. 2014, in prep). Initial tests indicate that the samples of RR Lyrae stars selected by our classification algorithm are highly pure ($\gtrsim 95\%$) and at least 95% complete within 80 kpc.

We note that the completeness tests were done assuming $R = 20.6$ mag as the 5σ detection limit for PTF (Law et al. 2009), which assumes $2''$ seeing and no clouds. Since not all PTF observations were done in such conditions, the true completeness will vary as a function of the sky position. For example, PTF fields observed during summer months will be deeper and have better photometry than fields observed during winter months, when the atmospheric conditions are less favorable. A completeness map for RRab stars identified by PTF that takes into account various selection effects (survey cadence, depth of specific fields), will be released in the upcoming paper (Banholzer et al. 2014, in prep).

For this work, we limit our sample of RRab stars to those with heliocentric distances greater than 60 kpc, for three reasons. First, halo structures (e.g., dSphs) located at greater heliocentric distances are more likely to remain spatially coherent for a longer time due to longer orbital periods. Second, the number density profile of RR Lyrae stars declines more steeply beyond ~ 30 kpc from the Galactic center (Watkins et al. 2009; Sesar et al. 2010). The consequence of this steepening is a reduction in the number of RR Lyrae stars beyond 30 kpc that are likely associated with the smooth stellar spheroid (e.g., see Figure 11 of Sesar et al. 2010 for an illustration). By considering only distant RR Lyrae stars, we minimize the number of RR Lyrae stars that are likely associated with the smooth halo (and not associated with potential dSphs) and therefore minimize the background in our search. And third, according to Tables 2 and 3 of Koposov et al. (2008), blind searches based on SDSS data have likely found all Segue 1-like dSphs within ~ 45 kpc from the Sun. Thus, further searches in the SDSS footprint and within 45 kpc from the Sun are not likely to uncover new dSphs.

In total, our sample consists of 123 RRab stars that cover 9000 deg^{-2} of sky and are located within 60 to 100 kpc from the Sun. Their distribution in equatorial coordinates is shown in Figure 1 (*left*) and their positions are listed in Table 1. We removed RR Lyrae stars associated with known dSphs or globular clusters. The

⁸ <http://www.ptf.caltech.edu>

⁹ The Mould- R filter is similar in shape to the SDSS r -band filter, but shifted 27 Å redward.

RRab stars within 9° off the orbital plane of the Sagittarius stream are more likely to be associated with the stream than with a low-luminosity dSph, and were thus excluded from our sample. The period vs. amplitude diagram (right panel of Figure 1) shows the distribution of RRab stars according to the Oosterhoff classification (Oosterhoff 1939, or see Section 5.1 of Zinn et al. 2014 for a brief review). We find the ratio of Oosterhoff type I and II RRab stars to be 4 : 1. The same ratio was also found by previous studies that used samples of closer RR Lyrae stars (Miceli et al. 2008; Drake et al. 2013; Sesar et al. 2013a; Zinn et al. 2014).

3. DETECTION METHOD

3.1. Basis of the Method

While only a few HB and RGB stars may be observable in a distant low-luminosity dSph, these stars should be located in the vicinity of a distant RRab star¹⁰. By converting the positions of stars near the RRab star to a coordinate system where the RRab star is in the center, and by stacking many stars from different sightlines (all centered on different RRab stars), one may hope to find a statistically significant overdensity of sources near the origin of this coordinate system, indicating a statistical detection of low-luminosity dSphs. Naturally, this signal may be detectable only if a sufficient fraction of sightlines contains a dSph (see Section 3.3 for a discussion). A flowchart of the detection method is shown in Figure 2 and described below.

First, we select a distant RRab star from our RRab sample, with a heliocentric distance between 60 and 100 kpc. We then select all SDSS point sources brighter than $r = 21.5$ mag¹¹ and within $30'$ of the position of the RRab star. To avoid creating an overdensity consisting only of RRab stars, we ignore sources within $1''$ of the position of the RRab star. The SDSS morphological star-galaxy classification is reliable for sources brighter than $r = 21.5$ (Lupton et al. 2002), and thus we expect little or no contamination from unresolved galaxies.

To select candidate RGB stars at the distance indicated by the RRab star, we compare positions of SDSS sources in the $g - r$ vs. r color-magnitude diagram¹² with a theoretical BaSTI¹³ isochrone (Pietrinferni et al. 2006), shifted using the distance modulus of the RRab star (i.e., we do color-magnitude diagram filtering; Grillmair et al. 1995). More specifically, we use the isochrone of an old (12.6 Gyr), metal-poor ($[Fe/H] = -2.1$ dex), α -enhanced population, with an assumed mass loss parameter $\eta = 0.4$.

In practice, we require that a source's $g - r$ color is within $2\sigma_{g-r}$ or 0.2 mag from the isochrone, where σ_{g-r} is the uncertainty in $g - r$ color. Following Walsh et al. (2009, see their Section 3.2), we remove sources with $g - r > 1.0$, as including redder objects adds more noise from Milky Way dwarf stars than signal from more dis-

tant RGB stars. Similarly to candidate RGB stars, candidate blue horizontal branch (BHB) stars are selected by comparing dereddened g -band magnitudes of SDSS sources against a fiducial BHB line defined by Fermani & Schönrich (2013, Equation 5).

The angular positions of selected sources relative to the position of the RRab star, $\Delta RA = (RA - RA_{RRab}) \cos((Dec + Dec_{RRab})/2)$ and $\Delta Dec = Dec - Dec_{RRab}$, are converted to projected (physical) positions $\Delta x = \Delta RA \cdot d$ and $\Delta y = \Delta Dec \cdot d$, where d is the heliocentric distance of the RRab star. Only sources within the projected distance of $\sqrt{\Delta x^2 + \Delta y^2} < 500$ pc from the RRab star are kept.

The above selection procedure is repeated for 123 sightlines centered on 123 RRab stars. Sources from each sightline that pass the selection are collected and their projected positions are stored.

3.2. Maximum Likelihood Estimation of the Significance of Detection

To test for the presence of an overdensity of sources near the origin of the Δx vs. Δy coordinate system, we use the maximum likelihood approach of Martin et al. (2008, see their Section 2.1).

We model the spatial distribution of sources in the Δx vs. Δy plane with an axially symmetric exponential radial density profile centered on the origin and superposed on a uniform field contamination. Given this spatial model, the probability of finding a data point i at distance $r_i = \sqrt{\Delta x_i^2 + \Delta y_i^2}$ from the origin is

$$P_i(r_i|N^*, r_e) = \frac{2\pi r_i}{N_{tot}} \left(\frac{N^*}{2\pi r_e^2} \exp\left(-\frac{r_i}{r_e}\right) + \Sigma_b \right), \quad (1)$$

where N^* is the number of stars (in the stack) that belong to low-luminosity satellites, r_e is the exponential scale radius of the profile (half-light radius is $r_h = 1.68r_e$), and Σ_b is the surface density of foreground stars (in units of stars pc^{-2})

$$\Sigma_b = \frac{N_{tot} - N^*}{r_{max}^2 \pi}. \quad (2)$$

In Equations 1 and 2, N_{tot} is the total number of sources in the stack and $r_{max} = 500$ pc.

Given a spatial distribution of a set (\mathcal{D}_n) of N_{tot} points, the likelihood of the entire data set is

$$\mathcal{L}(\mathcal{D}_n|N^*, r_e) = \prod_{i=1}^{N_{tot}} P_i(r_i|N^*, r_e). \quad (3)$$

The probability of a model given the data, $P(N^*, r_e)$, is then

$$P(N^*, r_e|\mathcal{D}_n) \propto \mathcal{L}(\mathcal{D}_n|N^*, r_e) P(N^*) P(r_e), \quad (4)$$

where $P(N^*) = 1/2000$ for $0 < N^*/\text{stars} < 2000$ and $P(r_e) = \mathcal{N}(\log(r_h = 1.68r_e)|\mu = 2.26, \sigma = 0.8)$ is a normal distribution in $\log(r_h = 1.68r_e \text{ pc}^{-1})$, centered on $\mu = 2.26$ and with a standard deviation of $\sigma = 0.8$ ($P(r_e) = 0$ for $r_e \leq 0$ pc).

We chose a flat prior for N^* because we expect $\lesssim 10$ RGB and HB stars per sightline and have 123 sightlines in the stack (a sightline with a dSph that has much more

¹⁰ Of course, this idea works only if RRab stars trace positions of low-luminosity dSph in the first place. The fact that almost every known low-luminosity dSph has an RR Lyrae star (see Section 1), supports this assumption.

¹¹ In this work, we use SDSS point-spread function (PSF) magnitudes.

¹² From here on, all SDSS colors and magnitudes are dereddened using dust maps of Schlegel et al. (1998)

¹³ <http://basti.oa-teramo.inaf.it/>

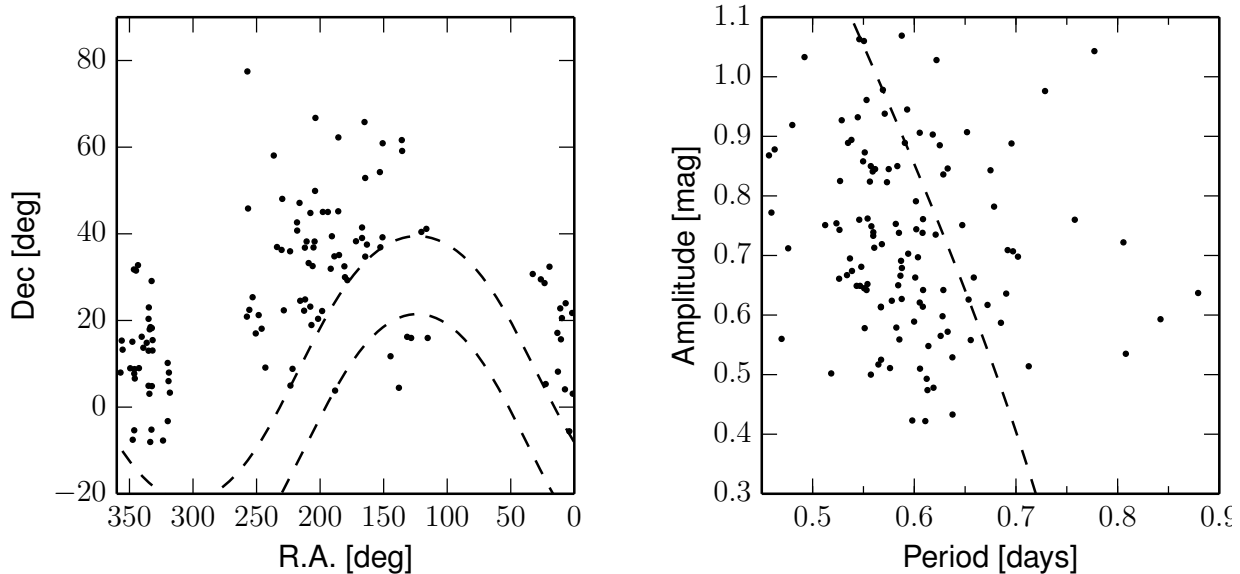


Figure 1. *Left:* The angular distribution of RRab stars used in this work. The dashed lines show $\pm 9^\circ$ off the Sagittarius stream orbital plane. There are about 60 RRab stars within this region that were not included in our sample. *Right:* The distribution of selected RRab stars in the period vs. amplitude diagram. The dashed line (defined by Sesar et al. 2013a, see their Section 4) separates Oosterhoff type I (short-period) from type II (long-period) RRab stars.

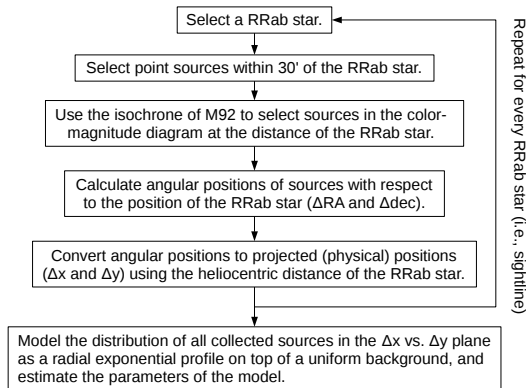


Figure 2. A flowchart of our detection method.

than 10 stars would likely be luminous enough to be detected by now). Thus, the expected number of dSph stars in the stack (N^*) may range from 0 to $\lesssim 2000$ ($\sim 10 \times 123 \lesssim 2000$).

The prior probability $P(r_e)$ has been chosen based on the size-luminosity relation for Milky Way dSph satellites (Brasseur et al. 2011). The center μ of the normal distribution $\mathcal{N}(\log(r_h))$ was calculated using Equation 9 of Brasseur et al. (2011) and assuming $M_V = -2$. We have adopted a wider normal distribution than Brasseur et al. (2011) (0.8 dex vs 0.2 dex) to account for smaller and less luminous dSphs (i.e., similar to Segue 1) that could have been biased against in the Brasseur et al. (2011) study (due to the surface brightness detection limit of SDSS).

The probability of the model described by Equation 4 is evaluated on a grid of (N^* , r_e) values. The pair of (N^* , r_e) values that yields the highest value of $P(N^*, r_e | \mathcal{D}_n)$ represents the model most favored by data. However, more important is to know whether this model is significantly better than the model that contains no low-luminosity galaxies in the stack (i.e., the model where $N^* \rightarrow 0$). As discussed by Martin et al. (2013, see their Section 3.3.3), this information hinges on the prob-

ability of the model marginalized over all parameters but N^* , or in our case, marginalized over the grid in r_e ,

$$P_{N^*}(N^* | \mathcal{D}_n) \propto \int_{1 \text{ pc}}^{201 \text{ pc}} P(N^*, r_e | \mathcal{D}_n) dr_e. \quad (5)$$

Assuming that P_{N^*} follows the normal distribution, the favored model $\max(P_{N^*})$ deviates from the model with no low-luminosity dSph galaxies by S times its dispersion (i.e., a “S-sigma detection”) for S defined as (Martin et al. 2013)

$$S = \sqrt{2 \ln \left(\frac{\max(P_{N^*})}{P_{N^*}(N^* \rightarrow 0)} \right)}. \quad (6)$$

In practice, we evaluate $P_{N^*}(N^* \rightarrow 0)$ at $N^* = 0.1$, which is a small enough number for N^* that it has a minimal impact on the calculation of the significance.

3.3. The Sensitivity of the Detection Method

In Sections 3.1 and 3.2, we described a method that aims to detect faint stellar structures (e.g., low-luminosity dSphs) by stacking stars located near distant RRab stars. In this Section, we test the method and quantify its sensitivity.

We test our detection method by applying it to mock catalogs of stars. These catalogs contain mock dSphs embedded in the SDSS DR10 imaging catalog, which serves as a realistic foreground and background for mock dSphs. The mock dSphs are created by randomly drawing a fixed number of stars from a synthesized old, metal-poor population. The creation of mock dSph galaxies is described in detail in Appendix B.

In total, 123 sightlines are generated, out of which a user-defined fraction (f_{dSph}) contain a mock dSph, while the remaining sightlines contain only sources from SDSS DR10. The selection and stacking of sources is applied to all sightlines, as described in Section 3.1, with one modification. Even though the exact distance to each

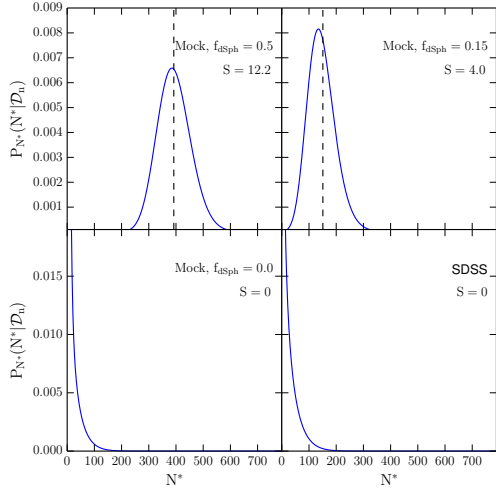


Figure 3. Marginal likelihood functions P_{N^*} for three mock catalogs with different fractions of dSphs (f_{dSph}), and for the SDSS DR10 catalog. The half-light radius of dSphs used in these mock catalogs is ~ 30 pc and their luminosity is $M_V = -1.5^{+0.6}_{-0.8}$. The significance S of detection is noted in each panel. For comparison, the dashed line shows the true N^* , measured from the mock sample with the background sources removed. Note the excellent agreement between the true value and the value of N^* where P_{N^*} peaks (i.e., the value of N^* favored by data).

mock dSph is known, this information is not used fully when doing the color-magnitude diagram filtering. To simulate the fact that in reality the distance modulus of RRab stars is uncertain at the 0.13 mag level ($\sim 6\%$ uncertainty in distance), a new distance modulus is drawn from a normal distribution that has a standard deviation of 0.13 mag and the mean equal to the true distance modulus. This distance modulus is then used when selecting sources in the $g-r$ vs. r color-magnitude diagram.

The performance of our detection method is demonstrated by Figure 3, which shows the marginal likelihood functions for three mock catalogs with different values of f_{dSph} . In these mock catalogs, the sightlines were populated by dSphs in order of the heliocentric distance, from the closest to the furthest (i.e., our “optimistic” scenario). Even though only a few stars are observable in each mock dSph (the vast majority are foreground stars), and even when only 18 out of 123 sightlines have a mock dSph ($f_{dSph} = 0.15$, top right panel), the favored model ($N^* \sim 150$) deviates from the model with no dSph galaxies by 4σ ($S = 4.0$), indicating a statistically significant detection.

While the results shown in Figure 3 are encouraging, it is important to remember that the mock dSphs are based on Segue 1, which has a half-light radius $r_h \sim 30$ pc (Martin et al. 2008). Distant dSphs that have a greater half-light radius than Segue 1 will be more difficult to detect. To test the sensitivity of our method to dSphs with the luminosity of Segue 1 ($M_V = -1.5^{+0.6}_{-0.8}$), but with a half-light radii greater than that of Segue 1 ($r_h \sim 30$ pc; Martin et al. 2008), we increase the size of mock dSph by some factor, create new mock catalogs, and then re-apply the detection method.

Figure 4 shows how the significance of detection changes as a function of f_{dSph} and the half-light radius

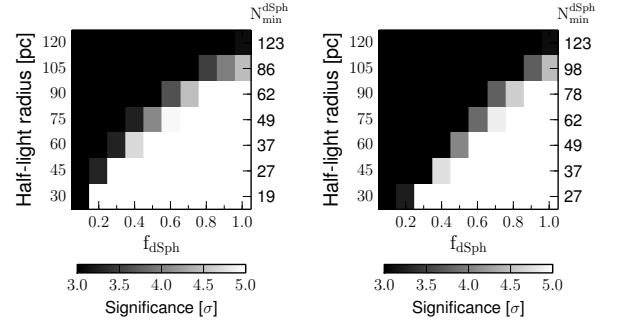


Figure 4. These panels show the regions of the parameter space where our method may or may not detect a signal, depending on the fraction of sightlines occupied by dSphs (f_{dSph}) and the half-light radius of dSphs. The significance of detection is expressed in units of standard deviation, σ , and is shown using a gray scale which saturates at 3σ and 5σ . Black pixels (significance $< 3\sigma$) show regions of the parameters space where we do not expect to be able to detect low-luminosity dSphs ($-2.7 < M_V < -1.5$) with high statistical significance. The left panel shows the results under the assumption that the closest f_{dSph} fraction of sightlines are populated by dSphs (the “optimistic” scenario), while the right panel shows the results under the assumption that the furthest f_{dSph} fraction of sightlines are populated by dSphs (the “pessimistic” scenario). The column of numbers next to each panel (N_{min}^{dSph}) lists the minimum number of dSphs needed in the stack to produce a 3σ detection, as a function of the half-light radius of dSphs in the stack.

of dSphs, for two different scenarios. As expected, as the half-light radius increases, the significance of detection decreases for a fixed f_{dSph} . That is, for our method to be able to detect the presence of more extended low-luminosity dSphs, more of the sightlines need to have a dSph. Based on Figure 4, we expect to be able to detect the presence of Segue 1-like low-luminosity dSphs if more than ~ 20 sightlines have a dSph (the bottom row of pixels in the left panel of Figure 4). The presence of low-luminosity dSph with half-light radii of ~ 120 pc will be detected only if every sightline has a dSph. Dwarf spheroidal galaxies with half-light radii greater than 120 pc and with luminosities $M_V = -1.5^{+0.6}_{-0.8}$ will likely not be detected.

We have repeated the above analysis for dSphs with the luminosity of Boötes 2 ($M_V = -2.7 \pm 0.9$), and have found the same sensitivity limits as the one shown in Figure 4 for Segue 1-like ($M_V = -1.5^{+0.6}_{-0.8}$) objects. While surprising at first, this result is not unreasonable given the uncertainties and overlap in M_V of Boötes 2 and Segue 1 dSphs.

4. APPLICATION TO THE SDSS DR10 IMAGING CATALOG

In this Section, we describe the application of our method to the SDSS DR10 imaging catalog. Three sets of sightlines are used to select sources from this catalog:

- Sightlines centered on 123 RRab stars located beyond 60 kpc from the Sun and 9° off the orbital plane of the Sagittarius tidal stream (i.e., our main set of sightlines).
- Sightlines centered only on Oosterhoff type II RRab stars.
- Sightlines centered at midpoints of close (< 200 pc) pairs of horizontal branch (HB) stars: RRab+RRab, RRab+BHB, or BHB+BHB star.

4.1. Main set of sightlines

Using the positions of 123 distant RRab stars as guiding centers, we have selected SDSS sources located in their vicinity and have repeated the stacking procedure described in Section 3.1.

As the bottom right panel of Figure 3 shows, the model favored by SDSS data is the one where there is no overdensity of sources at the origin of the Δx vs. Δy coordinate system ($N^* = 0$). That is, *the presence of low-luminosity dSph galaxies is not detected*. The marginal likelihood function P_{N^*} for target fields (bottom right panel) is virtually identical to the one for background fields (i.e., fields offset 1° west from RRab stars, bottom left panel).

4.2. Sightlines with Oosterhoff II RRab stars

As Figure 3 of Boettcher et al. (2013) shows, metal-poor ($[\text{Fe}/\text{H}] < -2$ dex) low-luminosity dSph galaxies mainly contain Oosterhoff type II RRab stars (i.e., RRab stars with periods longer than 0.65 days). As our Figure 1 shows, our sample is dominated by Oosterhoff type I RRab stars.

If low-luminosity dSph galaxies predominantly contain Oo II RRab stars, it makes sense to consider a stack consisting only of sightlines centered on Oo II RRab stars. Using Figure 1, we have selected ~ 30 of such sightlines and have repeated our analysis. Still, no signal was detected.

4.3. Sightlines with pairs of HB stars

The lack of a detection could be due to a preponderance of disrupted structures in the Galactic halo (e.g., streams, shells, clouds; Johnston et al. 2008). The surface brightness of structures decreases as they are disrupted, and a stack of sightlines centered on RRab stars in disrupted structures is not likely to yield a detection.

The fraction of sightlines centered on disrupted structures may be reduced by considering only sightlines that contain two or more RRab stars in close proximity. Since the number density of RRab stars in the outer halo is very low, a detection of two or more RRab stars in close proximity (< 200 pc) could indicate the presence of a spatially coherent structure (e.g., a low-luminosity dSph). Similarly, a close pair consisting of an RRab and a BHB star or a pair of BHB stars, could serve the same purpose. Dwarf spheroidal galaxies are known to have both types of horizontal branch stars (e.g., Segue 1). In addition, BHB stars are expected to outnumber the RR Lyrae stars in metal-poor populations (the ratio of BHB and RR Lyrae stars in the field is $\sim 6 : 1$; Preston et al. 1991).

We have searched for close pairs of RR Lyrae stars in our extended sample. The extended sample includes RRab stars that are within 9° off the orbital plane of the Sagittarius tidal stream, and stars with heliocentric distances greater than 45 kpc (the main RRab sample used so far starts at 60 kpc). We have found only two pairs of RRab stars separated by less than 200 pc. To search for close pairs of BHB and RRab stars, we have cross-matched our extended sample with the catalog of photometrically-selected BHB stars of Smith et al. (2010). We have found 7 close pairs consisting of a BHB and an RRab star. A cross-match of the BHB catalog

Table 2
Upper limits on the number of $-2.7 < M_V < -1.5$ dSphs within 9000 deg^2 and 60 to 100 kpc from the Sun

r_h^a (pc)	Optimistic	Pessimistic
30	< 19	< 27
45	< 27	< 37
60	< 37	< 49
75	< 49	< 62
90	< 62	< 78
105	< 86	< 98
120	< 123	< 123

^a Half-light radius of dSphs in the stack.

with itself yielded 5 close pairs of BHB stars. We have applied our method to the 14 sightlines described above, but once again, no signal was detected.

We have experimented with various modifications to our detection method in order to see if a signal appears. We have allowed fainter sources to be considered by changing the magnitude cut from $r = 21.5$ to $r = 22.5$ mag. Instead of using a single isochrone for color-magnitude diagram filtering, we adopted five BaSTI isochrones that span a range of metallicities, from $[\text{Fe}/\text{H}] = -1.6$ dex to $[\text{Fe}/\text{H}] = -3.6$ dex. In the end, none of the modifications significantly changed the bottom right panel of Figure 3 or our main conclusion – the presence of low-luminosity dSph galaxies is not detected.

5. DISCUSSION AND CONCLUSIONS

Almost every known low-luminosity Milky Way dSph satellite galaxy contains at least one RR Lyrae star (Table 4 of Boettcher et al. 2013). This observation, and the fact that RR Lyrae stars can be easily identified in multi-epoch imaging, motivated us to do a *guided* search for low-luminosity dSph galaxies, using distant RRab stars as tracers of their possible locations.

We use positions and distances of RRab stars to select SDSS stars that may be located in their vicinity (most likely, RGB stars). Sky positions of selected stars are transformed to a physical coordinate system that is centered on RRab stars, and sources from multiple sightlines are collected into a stack. If a fraction of sightlines contains a low-luminosity dSph, an overdensity of sources in the center of the stack should exist. By using mock catalogs, we have shown that our method is able to detect the presence of dSph galaxies even if only ~ 20 sightlines contain a dSph as faint as Segue 1 ($M_V = -1.5$).

We have applied our method to 123 sightlines that contain RRab stars identified by the Palomar Transient Factory (PTF) survey. These stars are spread over 9000 deg^2 of sky and span heliocentric distances from 60 to 100 kpc. However, we have not detected a statistically significant signal that would indicate the presence of low-luminosity dSph galaxies in the stack. Various modifications of our method did not change this result. An analysis of sightlines centered on close pairs of horizontal branch stars (separated by < 200 pc), also did not yield a detection.

Since no signal was detected, the sensitivity limits (N_{min}^{dSph}) shown in Figure 4 represent the upper limits on the number of $-2.7 < M_V < -1.5$ dSphs in the 9000 deg^2 of sky and within 60 to 100 kpc from the Sun (Table 2).

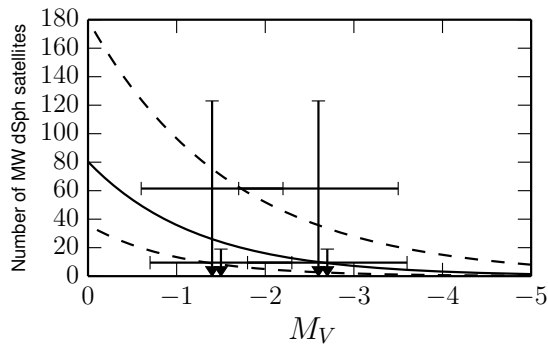


Figure 5. The solid line shows the estimated number of Milky Way dSph galaxies in the probed volume of the halo (9000 deg^2 and between 60 to 100 kpc from the Sun) based on the luminosity function of Tollerud et al. (2008). The dashed lines show the 1σ range of values. The symbols with error bars show the upper limits determined in this work, for galaxies with $M_V = -1.5 \pm 0.8$ (i.e., Segue 1-like) and $M_V = -2.7 \pm 0.9$ (i.e., Boötes 2-like), and with half-light radii of $r_h = 120 \text{ pc}$ and $r_h = 30 \text{ pc}$ (left and right arrow, respectively, for each M_V). We do not consider more luminous dSphs as such should have been already detected within 100 kpc in SDSS data (see Figure 10 of Koposov et al. 2008).

In Figure 5, we compare these upper limits with the luminosity function estimate of Tollerud et al. (2008). A comparison with the luminosity function estimate of Koposov et al. (2008) is not plotted, because Koposov et al. (2008) estimate that < 1 low-luminosity dSph should be present in the probed volume of the halo.

As Figure 5 shows, our upper limit on the number of $M_V \sim -1.5$ dSphs with $r_h = 30 \text{ pc}$ is slightly lower than the average estimate of Tollerud et al. (2008), though still within their 1σ range. If dSphs with such small half-light radii are remnants of tidally stripped galaxies, as some theoretical and observational studies speculate (Peñarrubia et al. 2008; Bovill & Ricotti 2011; Kirby et al. 2013), then our upper limit may constrain the efficiency and frequency of this process. The number of more extended dSphs (i.e., $r_h = 120 \text{ pc}$), is progressively less constrained. This is unfortunate, as some N-body simulations predict that the majority of low-luminosity dSphs should have $r_h > 100 \text{ pc}$ (e.g., Bovill & Ricotti 2011).

While we were not successful in detecting low-luminosity dSphs using the current sample of RR Lyrae stars identified by PTF, we hope to increase the volume of the probed Galactic halo by applying our method to sightlines centered on RR Lyrae stars identified using Pan-STARRS1 (PS1; Kaiser et al. 2010) multi-epoch data. While single-epoch PS1 images are not as deep as SDSS images, we are exploring the possibility that multi-band and multi-epoch PS1 data may be sufficient to enable detection of RRAb stars up to $\sim 130 \text{ kpc}$ from the Sun and over three quarters of the sky. Increasing the coverage of the PTF fields with sufficient epochs would also help. The increase in volume should allow us to more tightly constrain the luminosity function of Milky Way satellites and possibly measure the degree of (an)isotropy of their spatial distribution.

The prospects of detecting low-luminosity dSphs look even more exciting, once the multi-epoch data obtained by the Large Synoptic Survey Telescope (LSST; Ivezić et al. 2008) become available. Based on realistic simulations, LSST is expected to be able to detect $\geq 90\%$ of RRAb stars within $\sim 360 \text{ kpc}$ of the Sun across most

of survey footprint, and out to $\sim 760 \text{ kpc}$ in select deep fields (Oluseyi et al. 2012). At magnitudes corresponding to these distances ($r \sim 22.8$ and $r \sim 24.4$, respectively), galaxies dominate the source count and clusters of unresolved galaxies may become a non-negligible source of false-positive detections of dSphs. Advanced star-galaxy classification schemes will help with this issue (e.g., Fadelly et al. 2012), but actually *knowing* where a dSph may be and knowing its distance will be very useful. RRAb stars observed by LSST will provide that information, hopefully for a large fraction of yet to be discovered Milky Way satellites.

We thank Željko Ivezić, Erik Tollerud, and Colin Slater for comments, suggestions, and useful discussions. B.S and J.G.C thank NSF grant AST-0908139 to J.G.C for partial support, as do S.R.K (to NSF grant AST-1009987), and C.J.G (for a NASA grant). B.S acknowledges funding from the European Research Council under the European Unions Seventh Framework Programme (FP 7) ERC Grant Agreement n. [321035]. S.R.B thanks Caltech Summer Undergraduate Research Fellowship (SURF) for support. E.O.O. is incumbent of the Arye Dissentshik career development chair and is grateful to support by grants from the Willner Family Leadership Institute Ilan Gluzman (Secaucus NJ), Israeli Ministry of Science, Israel Science Foundation, Minerva foundation, Weizmann-UK foundation and the I-CORE Program of the Planning and Budgeting Committee and The Israel Science Foundation. This work has made use of BaSTI web tools.

This article is based on observations obtained with the Samuel Oschin Telescope as part of the Palomar Transient Factory project, a scientific collaboration between the California Institute of Technology, Columbia University, Las Cumbres Observatory, the Lawrence Berkeley National Laboratory, the National Energy Research Scientific Computing Center, the University of Oxford, and the Weizmann Institute of Science. It is also partially based on observations obtained as part of the Intermediate Palomar Transient Factory project, a scientific collaboration among the California Institute of Technology, Los Alamos National Laboratory, the University of Wisconsin, Millwakee, the Oskar Klein Center, the Weizmann Institute of Science, the TANGO Program of the University System of Taiwan, the Kavli Institute for the Physics and Mathematics of the Universe, and the Inter-University Centre for Astronomy and Astrophysics.

Funding for SDSS-III has been provided by the Alfred P. Sloan Foundation, the Participating Institutions, the National Science Foundation, and the U.S. Department of Energy Office of Science. The SDSS-III web site is <http://www.sdss3.org/>.

SDSS-III is managed by the Astrophysical Research Consortium for the Participating Institutions of the SDSS-III Collaboration including the University of Arizona, the Brazilian Participation Group, Brookhaven National Laboratory, Carnegie Mellon University, University of Florida, the French Participation Group, the German Participation Group, Harvard University, the Instituto de Astrofísica de Canarias, the Michigan State/Notre Dame/JINA Participation Group, Johns Hopkins University, Lawrence Berkeley National Labora-

tory, Max Planck Institute for Astrophysics, Max Planck Institute for Extraterrestrial Physics, New Mexico State University, New York University, Ohio State University, Pennsylvania State University, University of Portsmouth, Princeton University, the Spanish Participation Group, University of Tokyo, University of Utah, Vanderbilt University, University of Virginia, University of Washington, and Yale University.

REFERENCES

- Ahn, C. P., Alexandroff, R., Allende Prieto, C., et al. 2014, *ApJS*, 211, 17
- Belokurov, V., Zucker, D. B., Evans, N. W., et al. 2007, *ApJ*, 654, 897
- Boettcher, E., Willman, B., Fadely, R., et al. 2013, *AJ*, 146, 94
- Bovill, M. S., & Ricotti, M. 2011, *ApJ*, 741, 17
- Brasseur, C. M., Martin, N. F., Macciò, A. V., Rix, H.-W., & Kang, X. 2011, *ApJ*, 743, 179
- Cacciari, C., & Clementini, G. 2003, in *Lecture Notes in Physics*, Berlin Springer Verlag, Vol. 635, *Stellar Candles for the Extragalactic Distance Scale*, ed. D. Alloin & W. Gieren, 105–122
- Carlin, J. L., Grillmair, C. J., Muñoz, R. R., Nidever, D. L., & Majewski, S. R. 2009, *ApJ*, 702, L9
- Chaboyer, B. 1999, *Post-Hipparcos Cosmic Candles*, 237, 111
- Cordier, D., Pietrinferni, A., Cassisi, S., & Salaris, M. 2007, *AJ*, 133, 468
- Correnti, M., Bellazzini, M., & Ferraro, F. R. 2009, *MNRAS*, 397, L26
- Drake, A. J., Djorgovski, S. G., Mahabal, A., et al. 2009, *ApJ*, 696, 870
- Drake, A. J., Catelan, M., Djorgovski, S. G., et al. 2013, *ApJ*, 763, 32
- Fadely, R., Hogg, D. W., & Willman, B. 2012, *ApJ*, 760, 15
- Fermani, F., & Schönrich, R. 2013, *MNRAS*, 430, 1294
- Grillmair, C. J. 2009, *ApJ*, 693, 1118
- Grillmair, C. J., Freeman, K. C., Irwin, M., & Quinn, P. J. 1995, *AJ*, 109, 2553
- Ivezić, v., Tyson, J. A., Acosta, E., et al. 2008, *ArXiv e-prints*
- Johnston, K. V., Bullock, J. S., Sharma, S., et al. 2008, *ApJ*, 689, 936
- Kaiser, N., Burgett, W., Chambers, K., et al. 2010, in *Society of Photo-Optical Instrumentation Engineers (SPIE) Conference Series*, Vol. 7733, *Society of Photo-Optical Instrumentation Engineers (SPIE) Conference Series*
- Kirby, E. N., Boylan-Kolchin, M., Cohen, J. G., et al. 2013, *ApJ*, 770, 16
- Klein, C. R., Richards, J. W., Butler, N. R., & Bloom, J. S. 2011, *ApJ*, 738, 185
- Klypin, A., Kravtsov, A. V., Valenzuela, O., & Prada, F. 1999, *ApJ*, 522, 82
- Koch, A., Wilkinson, M. I., Kleyna, J. T., et al. 2009, *ApJ*, 690, 453
- Koposov, S., Belokurov, V., Evans, N. W., et al. 2008, *ApJ*, 686, 279
- Law, N. M., Kulkarni, S. R., Dekany, R. G., et al. 2009, *PASP*, 121, 1395
- Lupton, R. H., Ivezić, Ž., Gunn, J. E., et al. 2002, in *Society of Photo-Optical Instrumentation Engineers (SPIE) Conference Series*, Vol. 4836, *Survey and Other Telescope Technologies and Discoveries*, ed. J. A. Tyson & S. Wolff, 350–356
- Martin, N. F., de Jong, J. T. A., & Rix, H.-W. 2008, *ApJ*, 684, 1075
- Martin, N. F., Ibata, R. A., McConnachie, A. W., et al. 2013, *ApJ*, 776, 80
- Metcalfe, N., Farrow, D. J., Cole, S., et al. 2013, *MNRAS*, 435, 1825
- Miceli, A., Rest, A., Stubbs, C. W., et al. 2008, *ApJ*, 678, 865
- Moore, B., Ghigna, S., Governato, F., et al. 1999, *ApJ*, 524, L19
- Ofek, E. O., Frail, D. A., Breslauer, B., et al. 2011, *ApJ*, 740, 65
- Ofek, E. O., Laher, R., Law, N., et al. 2012a, *PASP*, 124, 62
- Ofek, E. O., Laher, R., Surace, J., et al. 2012b, *PASP*, 124, 854
- Oke, J. B., & Gunn, J. E. 1982, *PASP*, 94, 586
- Oluseyi, H. M., Becker, A. C., Culliton, C., et al. 2012, *AJ*, 144, 9
- Oosterhoff, P. T. 1939, *The Observatory*, 62, 104
- Peñarrubia, J., McConnachie, A. W., & Navarro, J. F. 2008, *ApJ*, 672, 904
- Perryman, M. A. C., de Boer, K. S., Gilmore, G., et al. 2001, *A&A*, 369, 339
- Pietrinferni, A., Cassisi, S., Salaris, M., & Castelli, F. 2006, *ApJ*, 642, 797
- Preston, G. W., Shectman, S. A., & Beers, T. C. 1991, *ApJ*, 375, 121
- Rau, A., Kulkarni, S. R., Law, N. M., et al. 2009, *PASP*, 121, 1334
- Reimers, D. 1975, *Memoires of the Societe Royale des Sciences de Liege*, 8, 369
- Schlegel, D. J., Finkbeiner, D. P., & Davis, M. 1998, *ApJ*, 500, 525
- Sesar, B., Ivezić, Ž., Lupton, R. H., et al. 2007, *AJ*, 134, 2236
- Sesar, B., Ivezić, Ž., Grammer, S. H., et al. 2010, *ApJ*, 708, 717
- Sesar, B., Ivezić, Ž., Stuart, J. S., et al. 2013a, *AJ*, 146, 21
- Sesar, B., Grillmair, C. J., Cohen, J. G., et al. 2013b, *ApJ*, 776, 26
- Simon, J. D., Geha, M., Minor, Q. E., et al. 2011, *ApJ*, 733, 46
- Smith, H. 2004, *RR Lyrae Stars*, Cambridge Astrophysics (Cambridge University Press)
- Smith, K. W., Bailer-Jones, C. A. L., Klement, R. J., & Xue, X. X. 2010, *A&A*, 522, A88
- Tollerud, E. J., Bullock, J. S., Strigari, L. E., & Willman, B. 2008, *ApJ*, 688, 277
- Walsh, S. M., Jerjen, H., & Willman, B. 2007, *ApJ*, 662, L83
- Walsh, S. M., Willman, B., & Jerjen, H. 2009, *AJ*, 137, 450
- Walsh, S. M., Willman, B., Sand, D., et al. 2008, *ApJ*, 688, 245
- Watkins, L. L., Evans, N. W., Belokurov, V., et al. 2009, *MNRAS*, 398, 1757
- Xue, X.-X., Ma, Z., Rix, H.-W., et al. 2014, *ApJ*, 784, 170
- York, D. G., Adelman, J., Anderson, Jr., J. E., et al. 2000, *AJ*, 120, 1579
- Zinn, R., Horowitz, B., Vivas, A. K., et al. 2014, *ApJ*, 781, 22

APPENDIX

RRAB STARS IN THE BOÖTES 2 AND BOÖTES 3 DSPH GALAXIES

Boötes 2 (Walsh et al. 2007) and Boötes 3 (Grillmair 2009) dSph galaxies are two low-luminosity dSphs ($M_V = -2.7 \pm 0.9$ (Martin et al. 2008) and $M_V = -5.8 \pm 0.5$ (Correnti et al. 2009), respectively) that are not listed in Table 4 of Boettcher et al. (2013) as having an RRab star. In order to verify whether these two dSphs truly lack RRab stars, we have searched our own sample of RRab stars (selected from PTF data) and the sample of RRab stars selected by Drake et al. (2013) from the Catalina Real-Time Sky Survey (CRTS; Drake et al. 2009).

We have found an RRab star near each of these dSphs and at an inferred distance comparable to that each of these two dSphs. Their light curves are shown in Figure 6 and their light curve properties, derived from fitting r -band templates of Sesar et al. 2010 to PTF and CRTS data, are listed in Table 3.

The RRab star near Boötes 2 is located 39 ± 2 kpc from the Sun within $1'.7$ off the center of Boötes 2. For comparison, the half-light radius of Boötes 2 is $r_h = 4'.2^{+1.1}_{-1.4}$ (Martin et al. 2008), and its heliocentric distance is 42 ± 2 kpc (Walsh et al. 2008). While we do not know the radial velocity of this RRab star, based on its position and distance we conclude that it is likely associated with the Boötes 2 dSph. Judging by its position in the period-amplitude diagram (Figure 1), this star is an Oosterhoff II RRab star. Using Figure 3 of Boettcher et al. (2013), which shows the mean

Table 3
RR Lyrae stars in Boötes 2 and 3

	Boö 2	Boö 3
R.A. (deg)	209.52935716	210.14384929
Dec (deg)	12.85634739	25.93130497
Survey	CSS	PTF
Period (days)	0.6332816	0.6332751
rHJD ₀ (days) ^a	55621.942645	55371.793948
Amplitude (mag)	0.99	0.94
m ₀ (mag) ^b	17.89	18.23
⟨m⟩ (mag) ^c	18.46	18.80
[Fe/H] (dex)	-1.79 ^d	-2.02
v_{helio} (km s ⁻¹) ^e	n.a.	173 ± 13
d_{helio} (kpc) ^f	39 ± 2	46 ± 2

^a Reduced Heliocentric Julian Date of maximum brightness (HJD - 2400000).

^b Magnitude at maximum brightness (not corrected for extinction).

^c Flux-averaged magnitude corrected for extinction.

^d Adopted from Koch et al. (2009).

^e Heliocentric velocity.

^f Heliocentric distance calculated assuming $M_{RR} = 0.23[\text{Fe}/\text{H}] + 0.93$ (Chaboyer 1999; Cacciari & Clementini 2003) as the absolute magnitude of an RR Lyrae star.

RRab period vs. mean [Fe/H] for Milky Way dwarf galaxies with predominately old stellar populations, we estimate that the metallicity of this RRab star may be between -2.5 and -2 dex.

The RRab star near Boötes 3 is located 46 ± 2 kpc from the Sun, and is offset $\sim 0^\circ.8$ east and south from the center of Boötes 3, in its “east lobe” (see Figure 10 of Grillmair 2009). The heliocentric distance of this star is equal to that of Boötes 3 (46 kpc; Grillmair 2009). Based on its position in the period-amplitude diagram (Figure 1), this star is an Oosterhoff II RRab star.

We observed this star on Aug 2nd 2013, using the Double Spectrograph (DBSP; Oke & Gunn 1982) mounted on the Palomar 5.1-m telescope. A 600 lines mm⁻¹ grating and a 5600 Å dichroic were used, providing a resolution of $R = 1360$ and a spectral range from 3800 Å to 5700 Å. The velocity and metallicity were measured following Sesar et al. (2013b, see their Sections 2.4 to 2.7).

The spectroscopic metallicity of this star, $[\text{Fe}/\text{H}] = -2.0 \pm 0.1$ dex, and its heliocentric center-of-mass velocity, $v_{helio} = 173 \pm 13$ km s⁻¹, are fully consistent with properties of Boötes 3; metallicity $[\text{Fe}/\text{H}] = -2.1 \pm 0.2$ dex, mean velocity $v_{helio} = 197.5 \pm 3.2$ km s⁻¹ and velocity dispersion $\sigma_v = 14.0 \pm 3.2$ km s⁻¹ (Carlin et al. 2009). The outlying position of this RRab star (in the “east lobe”) and its velocity relative to the dSph (173 vs. 198 km s⁻¹), suggest that the star may be part of a tidal stream extending from Boötes 3. If so, the proper motion of this star, which will be measured by the Gaia mission (Perryman et al. 2001), will be an important datum in any effort to constrain the orbit of this dSph galaxy.

CREATION OF MOCK DSPH GALAXIES

For an RRab star selected from our sample and located at RA_0 , Dec_0 , and heliocentric distance d , a mock dSph is created as follows. First, we randomly draw a fixed number of stars (N_{stars} , brighter than some absolute SDSS r -band magnitude M_r^{cut}) from an old (12.6 Gyr), α -enhanced, and metal-poor ($[\text{Fe}/\text{H}] = -2.3$ dex) population generated using the SYNTHETIC MAN population synthesis code (Cordier et al. 2007; available through the BaSTI web interface¹⁴). The Reimers (1975) mass loss parameter for this population is assumed to be $\eta = 0.4$, and the spread in metallicity is assumed to be $\sigma_{[\text{Fe}/\text{H}]} = 0.3$ dex.

Following discussions by Martin et al. (2008, see their Section 3) and Walsh et al. (2008, see their Section 3.6), we create mock dSphs with luminosity M_V by drawing N_{stars} brighter than some absolute SDSS r -band magnitude (M_r^{cut}). For example, Segue 1 dSph ($M_V = -1.5_{-0.8}^{+0.6}$ dex) has 70 stars brighter than $M_r = 4.2$ (Simon et al. 2011). Thus, when creating a mock dSph with $M_V = -1.5$, we randomly draw 70 stars brighter than $M_r^{cut} = 4.2$ from the synthetic population described above. Based on the analysis of Martin et al. (2008, see their Table 1), Boötes 2 dSph ($M_V = -2.7 \pm 0.9$) is estimated to have 37 stars¹⁵ brighter than $M_r = 3.9$ (corresponding to the magnitude limit of $r = 22$ at the heliocentric distance of 43 kpc for Boötes 2). Thus, when creating a mock dSph with $M_V = -2.7$, we randomly draw 39 stars brighter than $M_r^{cut} = 3.9$.

The next step is to spatially distribute drawn stars within the mock dSph. Since the sample of Segue 1 stars observed by Simon et al. (2011) represents the most complete sample of confirmed members of a dSph, we use the

¹⁴ http://basti.iaa-teramo.inaf.it/BASTI/WEB_TOOLS/synth_pop/index.html

¹⁵ For comparison, Martin et al. (2008) estimated that Segue 1 dSph has 65 ± 9 stars brighter than $r = 22$, well before Simon et al.

(2011) spectroscopically confirmed 70 Segue 1 stars up to the same magnitude limit.

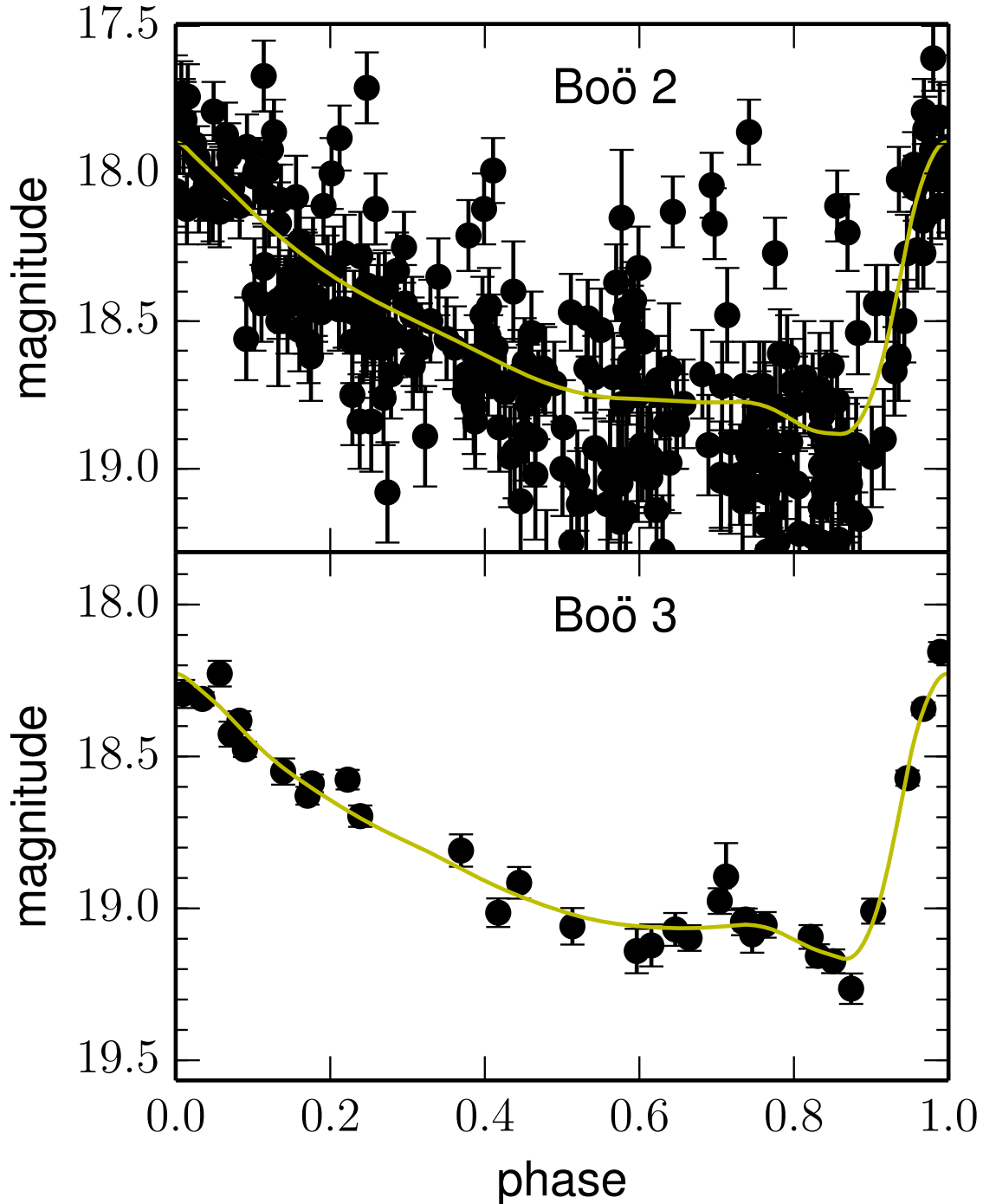


Figure 6. Phased light curves of RRab stars in the Boötes 2 (*top*) and Boötes 3 dSph galaxies (*bottom*), observed by CRTS and PTF, respectively. The solid lines show the best-fit *r*-band templates of Sesar et al. (2010).

spatial distribution of stars in Segue 1 as a template for the spatial distribution of stars in our mock dSph galaxies. To create this template spatial distribution, we first calculate the angular positions of spectroscopically confirmed members of Segue 1 relative to the center of Segue 1, as $\Delta RA = RA - RA_{Seg1}$ and $\Delta Dec = Dec - Dec_{Seg1}$. These angular positions are then converted to projected (physical) positions $\Delta x_{template} = \Delta RA \cdot d$ and $\Delta y_{template} = \Delta Dec \cdot d$, where $d = 23$ kpc is the heliocentric distance of Segue 1.

To spatially distribute drawn stars, we randomly assign them projected (physical) positions, $\Delta x_{template}$ and $\Delta y_{template}$, while making sure the same position is not assigned twice. A star in the mock dSph is then randomly selected and designated as the RRab star of the new mock dSph. The projected positions of other members are offset such that the mock RRab is placed in the center of the projected coordinate system, that is, $\Delta x = \Delta x_{template} - \Delta x_{RRab}$ and $\Delta y = \Delta y_{template} - \Delta y_{RRab}$. This translation of coordinates simulates the fact that for actual dSphs, the position

of the RRab star relative to the center of the dSph is not known. The Δx vs. Δy coordinate system is then rotated by some random angle, and the angular positions ΔRA and ΔDec are calculated using the heliocentric distance d of the observed RRab star.

Finally, the mock dSph is placed 1° west of the observed RRab star, along the same galactic latitude. This placement ensures that the foreground and background for the mock dSph are similar to the one at the position of the observed RRab star. At the same time, by slightly offsetting the mock dSph, we minimize the possibility of adding real dSphs into the mock catalogs, if such exist in the SDSS DR10 catalog at the positions of observed RRab stars.

In the final step, we modify the synthetic SDSS photometry of stars in the mock dSph. The apparent magnitudes are calculated using the heliocentric distance d of the observed RRab star and extinguished using dust maps of Schlegel et al. (1998). The photometric uncertainty is calculated using extinguished apparent magnitudes and models shown in Figure 1 of Sesar et al. (2007). The “observed” magnitude is then generated by drawing a value from a normal distribution that has a standard deviation equal to the photometric uncertainty and the mean equal to the extinguished apparent magnitude.